IEEE Access
Multidisciplinary | Rapid Review | Open Access Journal

Received July 23, 2019, accepted August 1, 2019, date of publication August 8, 2019, date of current version August 21, 2019.

Digital Object Identifier 10.1109/ACCESS.2019.2933895

Optimal Path Tracking Control of Autonomous Vehicle: Adaptive Full-State Linear Quadratic Gaussian (LQG) Control

KIBEOM LEE[1], SEUNGMIN JEON[1], HEEGWON KIM[2], AND DONGSUK KUM[1], (Member, IEEE)
[1]The Graduate School of Green Transportation, Korea Advanced Institute of Science and Technology (KAIST), Daejeon 34141, South Korea
[2]Autonomous Driving Development Group, Hyundai Motor Company (HMC), Hwaseong-si 16082, South Korea

Corresponding author: Dongsuk Kum (dskum@kaist.ac.kr)

This work was supported in part by Hyundai Motor Company in the South Korea under the University-Industry Collaborative Research Project 2018, and in part by the Technology Innovation Program under Grant 10083646 (Development of Deep Learning-Based Future Prediction and Risk Assessment Technology considering Inter-vehicular Interaction in Cut-in Scenario), funded by the Ministry of Trade, Industry, and Energy, South Korea.

ABSTRACT In practice, many autonomous vehicle developers put a tremendous amount of time and efforts in tuning and calibrating the path tracking controllers in order to achieve robust tracking performance and smooth steering actions over a wide range of vehicle speed and road curvature changes. This design process becomes tiresome when the target vehicle changes frequently. In this study, a model-based Linear Quadratic Gaussian (LQG) Control with adaptive Q-matrix is proposed to efficiently and systematically design the path tracking controller for any given target vehicle while effectively handling the noise and error problems arise from the localization and path planning algorithms. The regulator, in turn, is automatically designed, without additional efforts for tuning at various speeds. The performance of the proposed algorithm is validated based on KAIST autonomous vehicle. The experimental results show that the proposed LQG with adaptive Q-matrix has tracking performance in both low (15kph) and high (45kph) speed driving conditions better than those of other conventional tracking methods like the Stanley and Pure-pursuit methods.

INDEX TERMS Autonomous vehicle, intelligent vehicle, linear quadratic Gaussian (LQG) control, look-ahead distance, path tracking.

I. INTRODUCTION

Due to the increasing demand for safe and convenient vehicles, autonomous driving technology has been rapidly developed and some basic autonomous technologies, including the advanced driver assistant system (ADAS) have been commercialized and used by consumers [1], [2]. Autonomous driving technology brings together various fields of technology, but tracking a given path is not only the most basic function of autonomous vehicles, but also the most important function. As a tracking method in the early stage of development, tracking global GPS waypoints that have already determined is generally used. Based on this approach, path tracking controllers have been developed and used to follow basic roads or to complete a given mission.

The associate editor coordinating the review of this manuscript and approving it for publication was Jianyong Yao.

However, because autonomous driving technology has developed and become more sophisticated, it is necessary to track desired paths as they change in real time according to the surrounding situation. For example, lane change assist (LCA) or evasive steering assist (ESA) generates avoidance paths in real time according to changes in lane or surrounding obstacles [3]–[5]. Unlike the simple tracking control problem, which follows an existing path, the advanced tracking problem for autonomous vehicle should consider plant characteristics including error and noise problems in the path planning and localization stage. The controller used in an actual autonomous vehicle should be designed to take into account such plant problems.

In this way, the path tracking control has various considerations such as the characteristics of the plant, the tracking performance, and the ride comfort, and it is very difficult to design and tune the controller satisfying this. In reality, many autonomous vehicle developers put a tremendous amount of

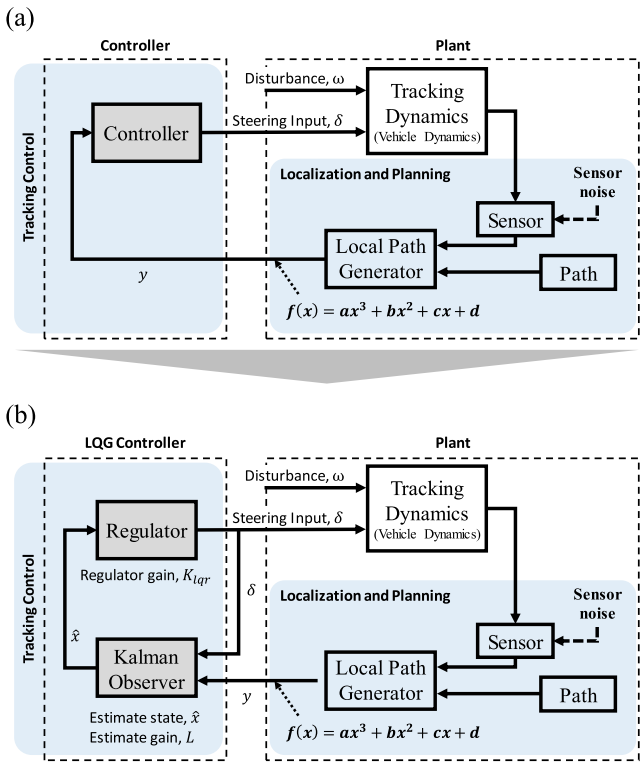

FIGURE 1. Control architecture for path tracking. (a) Conventional path tracking control architecture, (b) Proposed path tracking control architecture.

time and efforts in tuning and calibrating the path tracking controllers in order to achieve robust tracking performance and smooth steering actions over a wide range of vehicle speed and road curvature changes. Therefore, it is necessary to automatically design the controller that satisfying the target performance based on analyzed vehicle system.

In the literature, various algorithms for tracking control have been studied; the general tracking control architecture is shown in Fig. 1(a). The game approach, fuzzy algorithm, and neural-networks algorithm are used for tracking control [6]–[9]. The geometry based Stanley [10], [11] and Pure-pursuit [12]–[14] control methods have been proposed as the most popular algorithms; the output feedback control method based on the look-ahead concept has also been proposed [15]. These control methods have limited local path information that they can use because they are single input single output (SISO) systems. When a desired path is vibrating, the control gain has to be lowered to solve this problem. As a result, these controllers require a lot of tuning effort to reduce path vibrations and to improve tracking performance.

In the case of path tracking systems, the dynamic behavior and tracking characteristic change according to the vehicle driving speed. In the Stanley method, the vehicle speed term is included in the steering angle formula to compensate for characteristic differences. In Pure-pursuit, the look-ahead distance increases in proportion to the speed, so that changes in vehicle behavior characteristics can be complemented. However, since the behavior characteristics of the vehicle do not change in proportion to the speed, the problem cannot be completely solved by this equation. So, for vehicle implementation of this algorithm, the gain is tuned to an appropriate value according to the speed range. In the output feedback method, the look-ahead distance is appropriately tuned according to the speed. This tuning method has difficulty finding a value that yields adequate performance. In addition, tuning must be performed again if the vehicle or the vehicle parameters change.

A model-based controller such as kinematic or dynamic vehicle model is proposed to overcome the drawbacks of geometry or tuning-based algorithms. Model-based controllers can reduce the effort required for tuning because they are designed based on a model that has behavior similar to that of the vehicle [16]. Also, it is possible to solve the problem of characteristic change according to speed change because the model reflects vehicle driving characteristic changes. With these advantages, model-based controllers have been extensively studied [17]–[29]. Brown et al., Ji et al., Guo et al., and Cui et al. proposed model predictive control for path tracking [18]–[22]. Marino et al. and Zhao et al. proposed a method to design a PID controller based on the model [23], [24]. The design of the H-infinity controller was proposed by Hu et al. and Hu *et al.* [25], [26]. Cole et al., Xu et al., and Jiang et al. used state feedback with dynamic bicycle model [27]–[29]. In the case of the state feedback, it was possible to reflect the dynamic behavior in the vehicle model, but the tracking characteristics were not considered. In addition, since these controllers use part of the local path function, the tracking state information is limited. In previous research, the overall model-based controller lacked verification of the vehicle model before it was embedded in the vehicle. In addition, model lacked consideration of error and noise characteristics from the localization and path planning stage.

Therefore, the purpose of this study is design a full-state Linear Quadratic Gaussian (LQG) controller based on a verified vehicle model, considering both dynamic and tracking characteristics. Through this, the controller can be designed automatically without tuning. Using the LQG controller, it is possible to design an observer that reflects the error and noise characteristics in localization and planning; it is also possible to design a regulator considering the dynamic characteristics of the vehicle. This regulator and observer can isolate and solve the two problems that affect the system. In addition, because this method is based on the dynamic model, it is possible to quickly design a new controller with the same performance by updating the model parameters, even if the vehicle or the vehicle specifications change.

In the case of the LQG controller, however, the vehicle behavior characteristics that depend on the vehicle speed can be reflected through the dynamic model, but the tracking characteristic changes cannot be considered. The tracking characteristics change according to the speed and must be expressed through changes of the Q-matrix, which is a part of the cost function of the LQG controller. Changes of the Q-matrix can change the damping of the tracking

characteristic through the blending ratio of each vehicle state (e.g. lateral offset, heading offset). The tracking characteristics are theoretically analyzed and the appropriate look-ahead distance (Q-matrix in LQG) is found through the vehicle model. The adaptive Q-matrix ensures a similar tracking characteristic for various vehicle speeds and allows complete automation without need for tuning.

In this paper, a full-state LQG controller is designed to consider noise and error problems in the localization and planning stage, and to improve the ride quality. The adaptive Q-matrix, based on the look-ahead concept, is applied and it is found that this method can be used to design a controller automatically, without tuning at various speeds. The main contributions of this paper are: 1) To verify the vehicle model to be used through System Identification (ID). The verified model is used for theoretically analyze the driving characteristics and design the model based controller. 2) To find the tracking characteristics changes when the vehicle speed and look-ahead distance change. The look-ahead concept is introduced to design the Q-matrix of the LQG. Through this, the controller that maintains tracking characteristics such as damping (overshoot and time constant) can be designed even if the vehicle speed changes. 3) In order to compensate for the disadvantage of the center of gravity (CG) measurement point in LQG, an adaptive measurement point according to the vehicle speed is proposed. Finally, by comparison with other tracking algorithms, the performance improvement is confirmed.

The remainder of this paper is organized as follows: In Section II, a control architecture and vehicle modeling for controller design are proposed. System identification for model verification is carried out in section III. In section IV, an adaptive look-ahead distance is proposed. In section V, the LQG controller is designed. In section VI, designed controller performance evaluation is carried out with vehicle test. Finally, Section VI provides concluding remarks.

II. ARCHITECTURE OF TRACKING CONTROL AND VEHICLE MODELING

A. ARCHITECTURE OF TRACKING CONTROL

The proposed LQG controller architecture for path tracking is shown in Fig. 1(b). After taking the path information from the path planning stage, the correct vehicle state is estimated through the Kalman observer. Then, the optimal steering angle is calculated through the regulator. In order to improve the performance of the Kalman observer and the regulator, an accurate dynamic vehicle model is needed. Using an accurate vehicle model, observer is designed according to the sensor noise, and the regulator is designed using a cost function with an adaptive Q-matrix. The adaptive Q-matrix is designed according to the dynamic characteristics depending on the vehicle speed. In this way, it is possible to solve the error, noise, and vibration phenomena in the localization and path planning stages of autonomous vehicle.

The reference path information from the planning stage is transferred with a three-order function based on the vehicle body fixed coordinates, as shown as Eq. (1). The continuous gradient trajectory is good for tracking due to holonomic characteristics of vehicle. This three-order function method is generally used with many path planning algorithms and tracking devices (e.g. Mobileye).

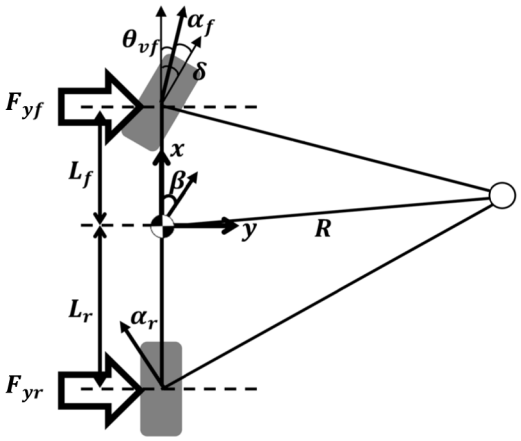

FIGURE 2. Vehicle lateral dynamics model (Bicycle model).

$$f(x) = ax^3 + bx^2 + cx + d \tag{1}$$

B. LATERAL DYNAMIC MODEL

The lateral dynamic model (bicycle model) is shown in Fig. 2. Front and rear tire force equations are written as Eqs. (2) and (3) respectively. Lateral force and moment equations are written as Eqs. (4) and (5). Using Eqs. (2)-(5), the combined vehicle lateral dynamics models are shown in Eqs. (6) and (7).

$$F_{yf} = 2C_{af}\left(\delta - \theta_{vf}\right) = 2C_{af}\alpha_f \tag{2}$$

$$F_{yr} = 2C_{ar}\left(-\theta_{vr}\right) = 2C_{ar}\alpha_r \tag{3}$$

$$m\left(\ddot{y} + \dot{\psi}V_x\right) = F_{yf} + F_{yr} \tag{4}$$

$$I_z\ddot{\psi} = l_f F_{yf} - l_r F_{yr} \tag{5}$$

$$\ddot{y} = -\left\{\frac{2C_{\alpha f}+2C_{\alpha r}}{mV_x}\right\}\dot{y} - \left\{V_x + \frac{2C_{\alpha f}l_f + 2C_{\alpha r}l_r}{mV_x}\right\}\dot{\psi} \tag{6}$$

$$\ddot{\psi} = -\left\{\frac{2C_{\alpha f}l_f - 2C_{\alpha r}l_r}{I_z V_x}\right\}\dot{y} - \left\{\frac{2C_{\alpha f}l_f^2 + 2C_{\alpha r}l_r^2}{I_z V_x}\right\}\dot{\psi} + \frac{2C_{\alpha f}l_f}{I_z}\delta \tag{7}$$

where F_{yf} and F_{yr} are the lateral force at the front tire and rear tire, respectively, l_f is the distance of the front axle from vehicle CG, l_r is the distance of the rear axle from vehicle CG, L is the wheel base, δ is the steering angle, α_f and α_r are the slip angle of the front and rear tires, R is the radius of the road curve, Ψ is the vehicle heading angle, β is the vehicle slip angle, θ_{Vf} and θ_{Vr} are the velocity angle of the front and rear tires, and $C_{\alpha f}$ and $C_{\alpha r}$ are the cornering stiffness values of the front and rear tires.

C. PATH TRACKING MODEL

A path tracking model is designed based on the lateral dynamic model using offsets of the desired path. The detailed

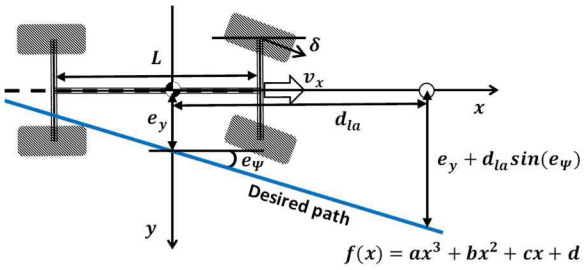

FIGURE 3. Path tracking system model with look-ahead concept.

meaning of each parameter is shown in Fig. 3. The lateral and heading offset rates are written as Eqs. (8) and (9), respectively.

$$\dot{e}_y = \dot{y} + V_x(\Psi - \Psi_{req}) \tag{8}$$

$$e_\Psi = (\Psi - \Psi_{req}) \tag{9}$$

The discrete path tracking system model is written as Eq. (10), as shown at the bottom of the next page. The discrete state space model is written as Eq. (11), as shown at the bottom of the next page. Vector $X = \left[e_y \ \dot{e_y} \ e_\Psi \ \dot{e_\Psi} \right]'$ represents the state variables of the system, and vector u $= [\delta]$ is the control inputs. where e_y is the distance of the vehicle CG from the desired path (lateral offset), $\dot{e_y}$ is the derivative of lateral offset, e_Ψ is the orientation error of the vehicle with respect to the desired path, $\dot{e_\Psi}$ is the derivative of the heading angle, Ψ_{req} is the required yaw angle, d_{la} is the look-ahead distance, y is the lateral offset at look-ahead point, and u is the control input.

In error dynamics systems, the lateral and heading offset states correspond to 'd' and 'c' from reference path $f(x)$, as shown in Eq. (1). The lateral and heading offset rate states correspond to 'c' and '2b' from $f(x)$. By using the third-order local path equation, all states of the tracking model can be determined. In this way, a full-state feedback for path tracking control is enabled.

III. MODEL VALIDATION WITH SYSTEM IDENTIFICATION

System identification is performed to confirm the vehicle model and parameters used for the controller design. The modeling accuracy will be confirmed by comparing the frequency response obtained from the vehicle experiment with that obtained from the vehicle model. The sine sweep method is used for system identification. This method compares the magnitude and phase of the sine wave input and output when sine waves with various frequencies are into the system. In practice, the steering wheel angle input is used. But, for convenience of comparison with the vehicle model, the steering angle is calculated according to the steering gear ratio.

A. TEST VEHICLE AND MODEL PARAMTERS

The test vehicle for the experiment is an IONIQ Hybrid by the Hyundai Motor Company. A photo of the test vehicle is shown in Fig. 4. The measured vehicle parameters for the same model are shown in Table 1.

FIGURE 4. Test vehicle for experiment (KAIST Autonomous Vehicle).

TABLE 1. Test vehicle parameters.

	Parameter	Nominal Value
Speed	V_x (m/s)	5
Mass	m (kg)	1490
Moment of Inertia	I_z (kgm^2)	2600
Center of Gravity Point	l_f (m)	1.1
	l_r (m)	1.6
Cornering Stiffness	C_{af} (N/rad)	53000
	C_{ar} (N/rad)	53000

B. SINE SIGNAL INPUT WITH VARIANCE FREQUENCY

To verify the vehicle response characteristics, a sine wave with various frequencies is generated and into the steering angle. Since the sampling time(t_s) of the MicroAutoBox® used to control the vehicle is 0.02sec, the Nyquist frequency that can be measured is 155rad/s. The sine wave frequency that 0 to 155rad/s is generated within 20seconds. The generated frequency is Eq. (12) and the input frequency graph is described in Fig. 5(a). In order to verify the nonlinearity of the vehicle model, the input angle gain is changed to 0.26rad, 0.52rad, and 0.78rad, and the experiment is repeated two times for each steering angle. The steering angle input is written as Eq. (13) and described in Fig. 5(b).

$$f = \frac{t}{2} \times 2\pi(\frac{t}{8.1}) \tag{12}$$

$$\delta = angle * \sin(f * t) \tag{13}$$

C. SYSTEM RESPONSE

The time and frequency responses of the lateral offset are shown in Fig. 6. Response data are acquired from experiment with six iterations. The time response with variance of steering gain and frequency is shown in Fig. 6(a). The conversion of the results of time response to frequency response is described in Fig. 6(b). The transfer function, which converts

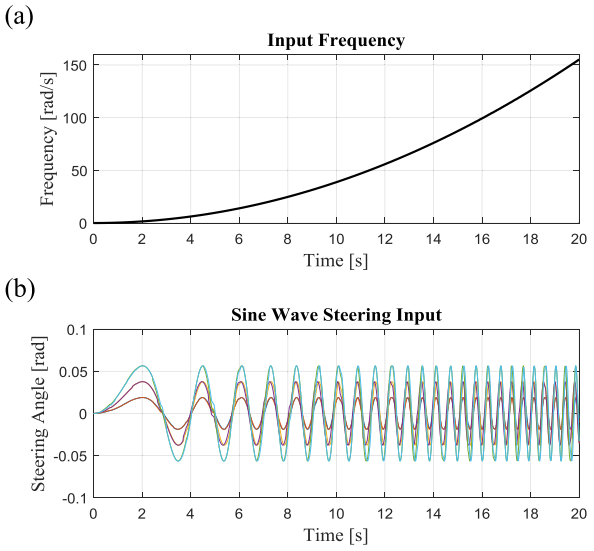

FIGURE 5. Sine signal input with variance frequency. (a) Input frequency over time. (b) Generated sinewave steering input according to modulation frequency.

the steering input to a lateral offset output, is estimated using the Matlab System Identification Toolbox. The estimated transfer function is written as Eq. (14) and shown in Fig. 6(b) as a blue dotted line. Since the transfer function in the bicycle model is quadratic, the system identification results are estimated in the same order. A comparison of system identification results and bicycle model results is shown in Fig. 6(c). In the high frequency regions, it is found that the results did not fit well, but the response was relatively accurate in the main control frequency region (blue region, [1 rad/s 10 rad/s]) of the vehicle.

$$\frac{e_y}{\delta} = \frac{-14.48s^3 + 6.452s^2 - 14.59s + 161.5}{s^4 + 8.419s^3 + 15.17s^2 + 22.68s + 7.891} \quad (14)$$

The time and frequency responses of the heading offset are shown in Fig. 7. Response data are acquired from an experiment with six iterations, the same process used to acquire the lateral offset results. The time response according to the variance of the steering gain and frequency is shown in Fig. 7(a). The conversion of the results of the time response to the frequency response is described in Fig. 7(b). The transfer function, using which the steering input is converted to lateral offset output, is estimated using the Matlab System Identification Toolbox. The estimated transfer function is written as Eq. (15) and shown in Fig. 7(b) as a blue dotted line. A comparison of system identification results and bicycle model results is shown in Fig. 7(c). In the high frequency regions, it is found that the results did not fit well, but the response was relatively accurate in the main control frequency region (blue region, [1 rad/s 10 rad/s]) of the vehicle.

$$\frac{e_\Psi}{\delta} = \frac{-2.191s^3 + 16.48s^2 + 39.57s + 21.72}{s^4 + 16.78s^3 + 23.74s^2 + 34.47s + 6.012} \quad (15)$$

In this section, the bicycle model and vehicle parameters to be used in the controller design are verified. The path tracking model that was designed in section II and the vehicle parameters in Table 1 will be used for adaptive look-ahead design and LQG controller design.

IV. ADAPTIVE LOOK-AHEAD DESIGN

The look-ahead concept is a method commonly used in lane keeping or path tracking systems. This concept can be used to control the driving characteristics of a vehicle on the basis of looking ahead, similar to how a person drives. The shorter the look-ahead distance is, the better the tracking performance will be; however, there will also be greater vibration of the vehicle. The longer the look-ahead distance is, the worse the tracking performance will be; there will also be less vibration, allowing higher passenger comfort. Because of these characteristics, the system has been tuned to increase the look-ahead distance as the speed increases. In state feedback, the look-ahead concept is expressed as the summation ratio of the lateral offset to the heading offset.

$$\begin{aligned} X_t &= AX_{t-1} + Bu_{t-1} + v \\ Y_t &= CX_t + w \end{aligned} \quad (10)$$

$$A = \begin{bmatrix} 1 & dt & 0 & 0 \\ 0 & 1 - \frac{2dt\left(C_{\alpha f} + C_{\alpha r}\right)}{mV_x} & \frac{2dt\left(C_{\alpha f} + C_{\alpha r}\right)}{m} & \frac{2dt\left(-C_{\alpha f} l_f + C_{\alpha r} l_r\right)}{mV_x} \\ 0 & 0 & 1 & dt \\ 0 & \frac{2dt\left(C_{\alpha f} l_f - C_{\alpha r} l_r\right)}{I_z V_x} & \frac{2dt\left(C_{\alpha f} l_f - C_{\alpha r} l_r\right)}{I_z} & 1 - \frac{2dt\left(C_{\alpha f} l_f^2 - C_{\alpha r} l_r^2\right)}{I_z V_x} \end{bmatrix}$$

$$\mathrm{B} = \begin{bmatrix} 0 \\ \frac{2dtC_{\alpha f}}{m} \\ 0 \\ \frac{2dtc_{\alpha f} l_f}{I_z} \end{bmatrix}, \quad \mathrm{C} = \begin{bmatrix} 1 & 0 & 0 & 0 \\ 0 & 1 & 0 & 0 \\ 0 & 0 & 1 & 0 \\ 0 & 0 & 0 & 1 \end{bmatrix} \quad (11)$$

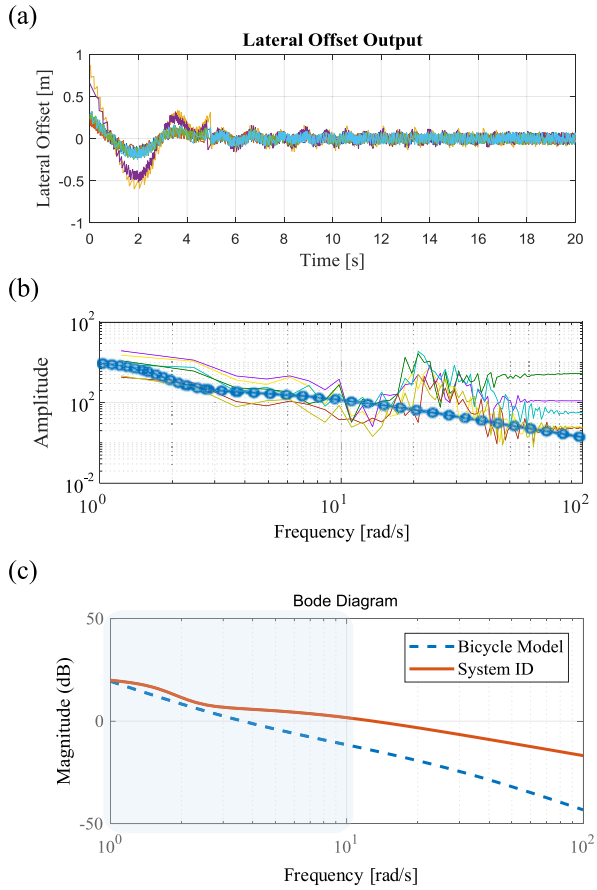

FIGURE 6. System response of lateral offset: (a) Time response, (b) Frequency response with identified data, and (c) Bode diagram with bicycle model and estimated transfer function.

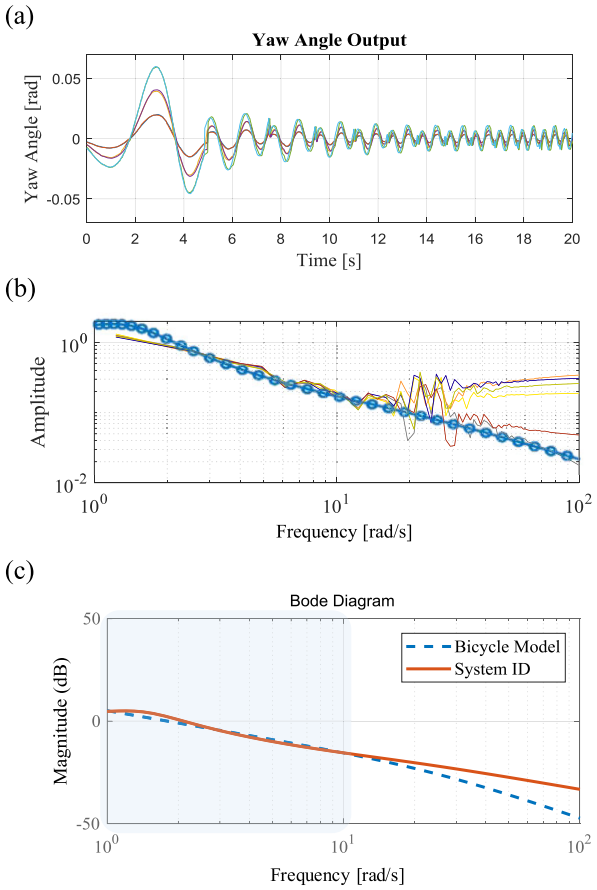

FIGURE 7. System response of heading offset: (a) Time response, (b) Frequency response with identified data, and (c) Bode diagram with bicycle model and estimated transfer function.

A. SYSTEM CHARACTERISTICS WITH VEHICLE SPEED AND LOOK-AHEAD DISTANCE

The path tracking characteristics are analyzed based on the bicycle and tracking model. The system input is the steering angle (δ) and the system output is the lateral offset at the look-ahead point ($e_y + d_{la} \cdot e_\Psi$) as written as Eqs. (10) and (16). It is possible to confirm the changes of the pole and zero while sweeping the vehicle speed and look-ahead distance.

$$Y = \begin{bmatrix} e_y \\ \dot{e_y} \\ e_\Psi \\ \dot{e_\Psi} \end{bmatrix}, \quad \mathrm{C} = \begin{bmatrix} 1 & 0 & 0 & 0 \\ 0 & 0 & 0 & 0 \\ 0 & 0 & d_{la} & 0 \\ 0 & 0 & 0 & 0 \end{bmatrix} \tag{16}$$

Figure 8(a) shows changes of pole and zero when the speed changes and while the look-ahead distance is fixed at 20m. The higher the speed, the closer the pole will move toward the imaginary axis. In the case of zero, the zero moves along the real axis when the speed gets faster. In the case of dominant zero, which has the greatest influence on the system characteristics, the real value decreases and the imaginary value increases as the speed increases. This means that vibration can occur when driving at a fast speed with short look-ahead distance. Figure 8(b) shows changes in pole and zero when the vehicle's speed is fixed at 30 m/s and the look-ahead distance is varied from 5 to 35. Changes of the look-ahead distance did not affect the pole, and when the look-ahead distance was large, it is confirmed that the zero is closer to the imaginary axis along the real axis.

The dominant zero tends to move away from the imaginary axis as the speed increases, and the dominant zero tends to approach the imaginary axis as the look-ahead distance becomes longer. This means that changing the look-ahead distance depending on the vehicle speed can fix the position of the dominant zero and keep the vehicle's characteristics the same even if the speed changes.

B. ADAPTIVE LOOK-AHEAD DESIGN

In Section IV A, the possibility of maintaining the tracking characteristics is confirmed for the designed look-ahead distance. When an autonomous vehicle follows a desired path, overshoot and vibration can have significant impacts on ride quality. When an autonomous vehicle is overdamped, it cannot converge quickly to the desired path. Therefore, it is important to find a critical damping point that can converge quickly on the path without overshoot or vibration. Figure 9(a) shows the result for the zero location while

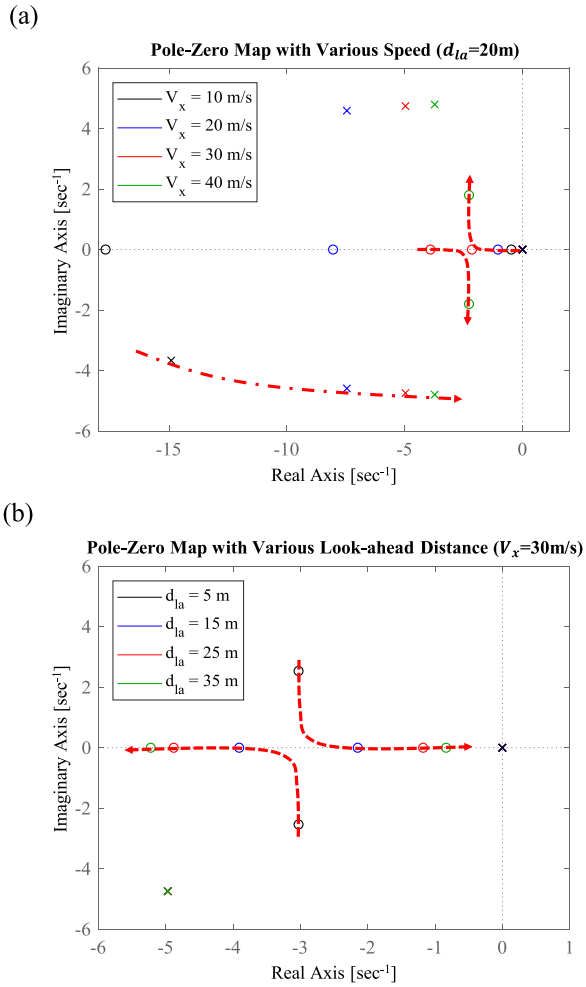

FIGURE 8. Pole-Zero map for various speeds and look-ahead distances. (a) Pole-Zero map for various vehicle speeds. (b) Pole-Zero map for various look-ahead distances.

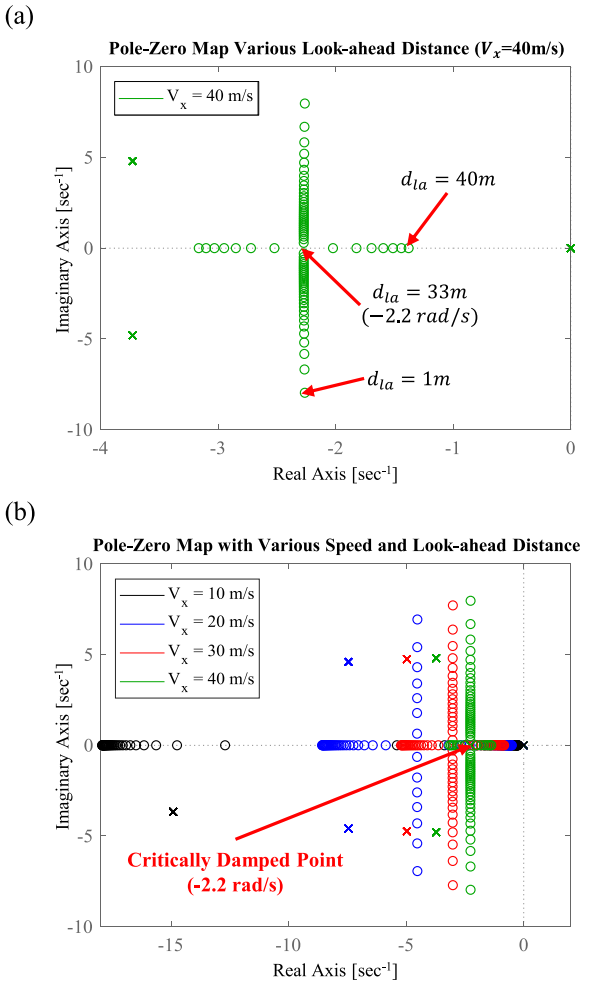

FIGURE 9. Pole-Zero map with sweeping look-ahead distance. (a) Pole-Zero map with look-ahead distance for distances of 0 to 40m at 40m/s speed. (b) Pole-Zero map with look-ahead distances of 0 to 40m at each speed.

sweeping the look-ahead distance from 1m to 35m at high speed (40m/s). This tracking system with speed of 40m/s is critically damped at −2.2rad/s, when the look-ahead distance is 20.4m.

The zero location is determined for various look-ahead distances and speeds. The results of the system characteristics are illustrated in Fig. 9(b). From these results, the look-ahead distance can be set to fix the path tracking characteristics of the vehicle at each speed. The look-ahead distance to fix the zero location at −2.2rad/s at each speed is shown in Table 2. The results, fitted with a quadratic equation according to the velocity, are written as Eq. (17).

$$d_{la} = 0.016 \times V_x^2 + 0.21 \times V_x - 0.32 \qquad (17)$$

The map of the tracking system Pole-Zero, with Eq. (17), which used the adaptive look-ahead distance, is provided in Fig. 10. The dominant zero is maintained at −2.2rad/s even if the vehicle speed changes. Therefore, using the proposed look-ahead distance, it is possible to control the vehicle with the same characteristics, even if the vehicle speed changes.

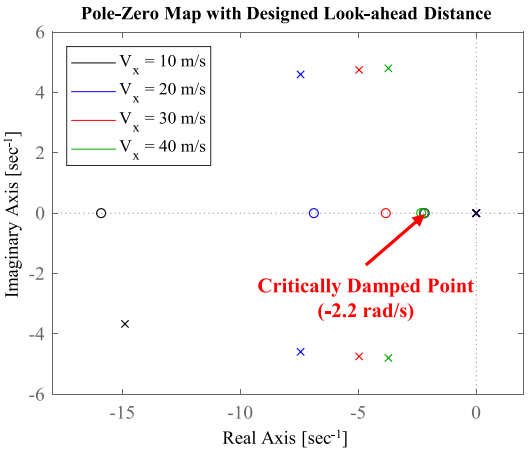

FIGURE 10. Pole-zero map with adaptive look-ahead distance.

V. LQG CONTROLLER DESIGN FOR PATH TRACKING

The full-state LQG controller is used for path tracking control. Since the local path equation has all states information of the tracking model, full-state controller can be designed.

TABLE 2. Desired look-ahead distance.

Vehicle Speed [m/s]	Desired Look-ahead Distance [m]
5	0.8
10	3.5
15	6.7
20	10.4
25	14.6
30	19.7
35	25.9
40	33.6

The LQG controller is a model-based controller that can be applied without manual tuning even if the vehicle plant changes. The regulator and observer design can solve the tracking problem and localization noise problem separately. Proposed LQG control architecture is shown in Fig. 1. In the previous section, section III, the bicycle model is confirmed to have characteristics similar to those of the actual vehicle in the region of interest. Therefore, the controller is designed based on the designed bicycle model and parameters.

A. REGULATOR DESIGN

When the linear control system is written as in Eq. (10), the LQR control input (K_{LQR}) can be expressed as Eq. (18).

$$u_{t-1} = -K_{LQR}X_{t-1} \tag{18}$$

The quadratic cost function to be minimized is described in Eq. (19). It is possible to determine the appropriate cost by setting the ratio of state and control gain through the ratio of Q to R. In this problem, the designed look-ahead distance is used as the ratio of the lateral offset (e_y) and heading offset (e_Ψ) to Q. The designed values of Q and R are given in Eq. (20).

$$J = \sum_{t=0}^{\infty} X_t^T Q X_t + u_t^T R u_t \tag{19}$$

$$\mathrm{Q} = \begin{bmatrix} 1 & 0 & d_{la} & 0 \\ 0 & 1 & 0 & 0 \\ d_{la} & 0 & d_{la}^2 & 0 \\ 0 & 0 & 0 & 1 \end{bmatrix} \mathrm{R} = 1 \tag{20}$$

The error covariance (P_{t+1}) is calculated using the Discrete Algebraic Riccati Equation (DARE), Eq. (21); the regulator gain (K_{LQR}) is calculated using the error covariance (P_{t+1}) in Eq. (22).

$$P_{t+1} = Q + A^T P_t A - A^T P_t B \left(B^T P_t B + R\right)^{-1} B^T P_t A \tag{21}$$

$$K_{LQR} = \left(B^T P_t B + R\right)^{-1} B^T P_t A \tag{22}$$

B. KALMAN OBSERVER DESIGN

The linear system with noise is described by Eq. (23). Y is the vector of the measured outputs available for feedback. In this problem, the measured outputs are the lateral and heading offset and the differentiated value of the lateral and heading offset. The vectors Y and C are described in Eq. (24).

Two noises affect the system: additive white Gaussian system noise v and white Gaussian measurement noise w.

$$\begin{aligned} X_t &= AX_{t-1} + Bu_{t-1} + v \\ Y_t &= CX_t + w \end{aligned} \tag{23}$$

$$Y = \begin{bmatrix} e_y \\ \dot{e_y} \\ e_\Psi \\ \dot{e_\Psi} \end{bmatrix}, \quad \mathrm{C} = \begin{bmatrix} 1 & 0 & 0 & 0 \\ 0 & 1 & 0 & 0 \\ 0 & 0 & 1 & 0 \\ 0 & 0 & 0 & 1 \end{bmatrix} \tag{24}$$

State($\hat{X}_t$) and output($\hat{Y}_t$) as estimated by an observer are described in Eq. (25). The observer estimates state X using the past step measurements and inputs. The matrix L is the Kalman observer gain.

$$\begin{aligned} \hat{X}_t &= A\hat{X}_{t-1} + Bu_{t-1} + L(Y_t - \hat{Y}_t) \\ \hat{Y}_t &= C\hat{X}_{t-1} \end{aligned} \tag{25}$$

The Kalman observer gain L is calculated using Eq. (26), and the noise information W and V to obtain the Kalman observer gain are described in Eq. (27). The values of W and V are tuned to meet the characteristics of this system (localization and path generation).

$$L = \Sigma_t C^T \left(C\Sigma_t C^T + W\right)^{-1} \tag{26}$$

$$W = \begin{bmatrix} 25 & 0 & 0 & 0 \\ 0 & 36 & 0 & 0 \\ 0 & 0 & 0.3 & 0 \\ 0 & 0 & 0 & 36 \end{bmatrix}, \; V = \begin{bmatrix} 1 & 0 & 0 & 0 \\ 0 & 1 & 0 & 0 \\ 0 & 0 & 1 & 0 \\ 0 & 0 & 0 & 1 \end{bmatrix} \tag{27}$$

Error covariance (Σ_t) for Kalman observer gain is determined by the following DARE equation, as described in Eq. (28) and Eq. (29).

$$\Sigma_{t+1} = A\Sigma_t A^T + V - A\Sigma_t C^T \left(C\Sigma_t C^T + W\right)^{-1} C\Sigma_t A^T \tag{28}$$

$$\Sigma_t = E[\left(x_t - \hat{x}_t\right)\left(x_t - \hat{x}_t\right)^T] \tag{29}$$

C. ADAPTIVE MEASURMENT POINT

In the previous section IV. B, the damping characteristic changed according to the look-ahead distance concept. This concept is applied to the LQG in the form of a Q-matrix. However, it has an effect similar to obtaining the forward information by using the ratio of the lateral and heading offset at the CG point of the current vehicle, rather than looking ahead [30]. For large curvature roads, this method provides limited information compared to the Stanley, Pure-pursuit, and Look-ahead tracking models, which measure offset at the front position. This drawback becomes worse as the curvature becomes larger and the vehicle speed faster. As the driving speed increases and steady state error occurs, it is necessary to improve the performance by moving the position of the measurement forward. The adaptive measurement point is described in Fig. 11; the equation is Eq. (30)

$$\mathrm{P_m}\left(V_x\right) = \begin{cases} 0 & (V_x < 4[m/s]) \\ \frac{1}{8}V_x - \frac{1}{2} & (4 \le V_x < 12[m/s]) \\ 1 & (12 \le V_x[m/s]) \end{cases} \tag{30}$$

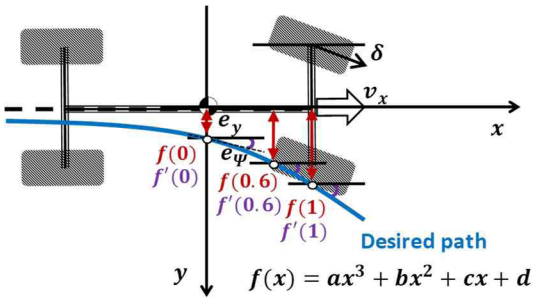

FIGURE 11. Adaptive measurement point concept.

VI. PERFORMANCE EVALUATION WITH VEHICLE EXPERIMENT

The designed controller is embedded in the autonomous test vehicle for performance evaluation. The designed path tracking system is tested under various test conditions and various vehicle speeds. Finally, the designed controller (LQG with adaptive Q-matrix (LQG)/LQG with adaptive Q-matrix + adaptive measurement point (LQG with AM)) is compared with other generally-used controllers (Stanley and Pure-pursuit).

A. VEHICLE SETTINGS

The architecture of the autonomous test vehicle is shown in Fig. 12. The desired path is given as GPS waypoints, and the position of the current vehicle is acquired through DGPS RTK. The local path (vehicle fixed coordinates) is generated based on the vehicle position and desired path. The designed controller is embedded in MicroAutoBox® and calculated steering angle command is sent to vehicle motor driven power steering (MDPS) module. Details of the model and specifications of DGPS RTK and MicroAutoBox® are provided in Table 3.

TABLE 3. Autonomous test vehicle system specifications.

	Parameter	Specification
DGPS RTK (Model: FlexPak6)	Position Accuracy (RMS)	1 cm + 1 ppm
	Data Rate	100 Hz
MicroAutoBoxII (Model: 1401/1513)	Processor	IBM PPC 750GL, 900 MHz
	Memory	16MB

B. DRIVING SCENARIOS FOR EXPERIMENT

The performance of the proposed controller is evaluated based on two scenarios. The first scenario is a double lane change (DLC) maneuver test, as shown in Fig. 13. The DLC is an ISO3880 evaluation criterion that is generally used to evaluate vehicle dynamics performance, like the electro stability program (ESP). Therefore, the DLC is a very severe test scenario for path tracking. The second scenario is a constant round test scenario, as shown in Fig. 14. This scenario starts

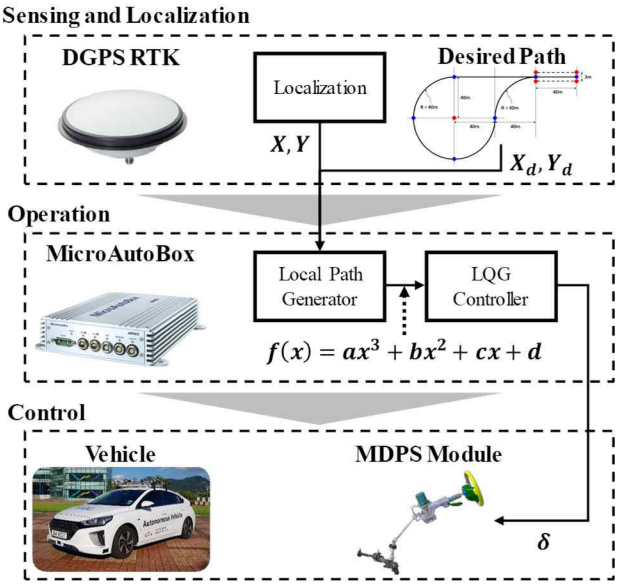

FIGURE 12. Test vehicle control architecture.

with a straight path; vehicle then enters a constant curvature, enters a reverse curvature, and then exits to a straight path again. This test scenario can evaluate the tracking performance of steady state error for severe curvature and severe curvature changes. The test is conducted under two vehicle speed conditions of 15kph and 45kph, with all controllers.

C. EXPERIMENT RESULTS

The results of each experiment are compared according to the lateral offset, heading offset, and steering angle. The results show how the tracking performance changes according to each set of experimental conditions and how much the designed part improves the performance. LQG with AM and LQG are compared to determine the effect of measurement position change on the tracking performance. Through comparison with the popular Stanley and Pure-pursuit methods, the performance difference between the model-based automatically designed controller and the tuning-based controller is determined. The Stanley and Pure-pursuit controllers were tuned a lot to achieve maximum controller performance. Detailed modeling of the Stanley and Pure-pursuit models is provided in the APPENDIX.

1) DOUBLE LANE CHANGE (DLC) TEST SCENARIO

The DLC scenario test results at 15kph are shown in Fig. 15. Because of the low-speed driving situation, all four controllers exhibit good performance, within 10cm lateral offset. LQG with AM and LQG show the same performance because the adaptive measurement point at 15kph is 0.

The DLC scenario test results at 45kph are shown in Fig. 16. As the speed increases, the performance of each controller varies depending on the controller characteristics. Since the DLC scenario is a very severe one of driving at 45kph, the lateral offset increases to 0.5m-1.0m.

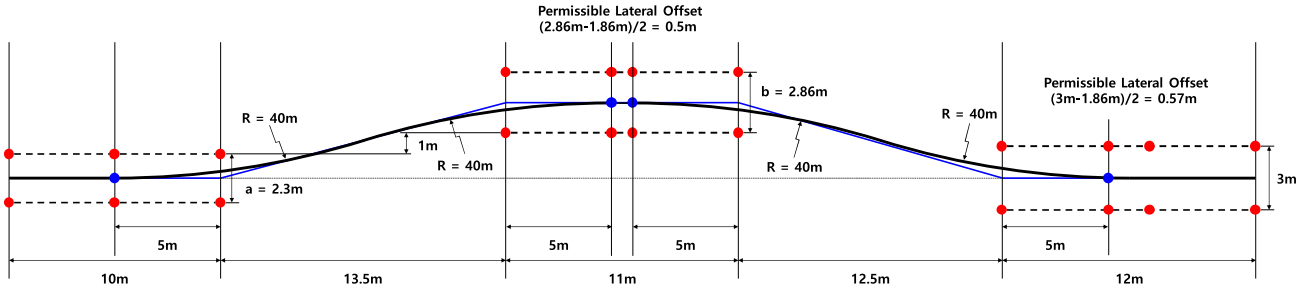

FIGURE 13. Double Lane Change Scenario for Performance Evaluation.

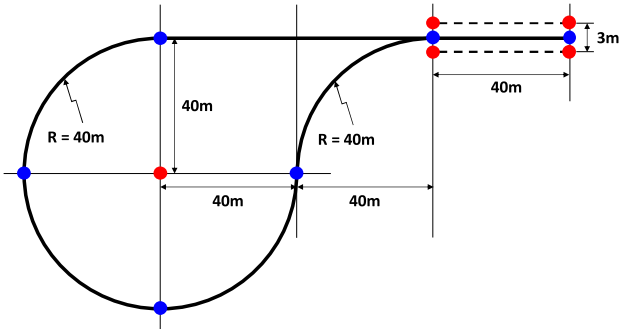

FIGURE 14. Constant round scenario for performance evaluation.

In the Stanley model, as the speed increases, $k_{stanley}$ does not fully respond to the change in speed, and the steering wheel trembles during tracking. The tracking performance is slightly lower than that of the LQG controller. In the case of the Pure-pursuit model, as the vehicle speed increases, the look-ahead distance becomes longer proportional to the speed. A long look-ahead distance leads to smooth driving without vibrations, but the tracking performance is poor. Also, when the vehicle leaves the desired path, the long look-ahead distance makes the time of recovery to the path longer. In the case of the LQG, the performance does not deteriorate with the change of the tracking and the vehicle model with proper speed. In the case of LQG with AM, the lateral offset is within 0.4m, the best performance among the controllers.

To quantitatively evaluate the performance of the controller, the peak lateral offset, the peak heading offset, and the peak steering speed are compared. The comparison results at each speed condition are shown in Fig. 17. As can be seen in the previous analysis, each controller has good and similar performance at low speed. All controllers controlled the lateral offset to within 0.1m. In the 45kph driving condition, the performance varies depending on the characteristics of the controllers.

In the case of the Pure-pursuit model, the peak lateral offset performance drops close to 1m and the peak steering speed is very low. For proper use of Pure-pursuit, rather than simply increasing the look-ahead distance in proportion to speed, look-ahead distance tuning is required for each speed section. In the case of the Stanley model, the peak lateral offset is 0.5m, which is similar to LQG. However, as the

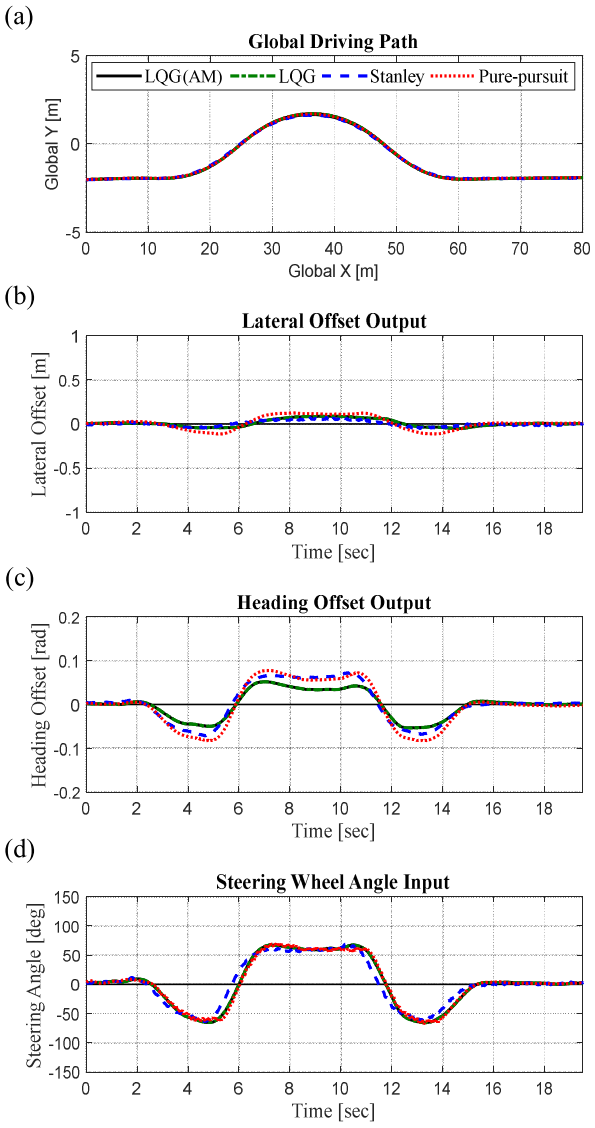

FIGURE 15. Tracking performance experiment results with designed LQG with forward measurement, LQG, Stanley, and Pure pursuit controllers for DLC test scenario (15kph). (a) Global driving path. (b) Lateral offset, (c) Heading offset, (d) Steering wheel angle.

speed increases, there is a slight difference in performance from the LQG. Therefore, it is predicted that the lateral offset performance of the Stanley model will deteriorate if the vehicle speed increases further. For LQG with AM, the steady

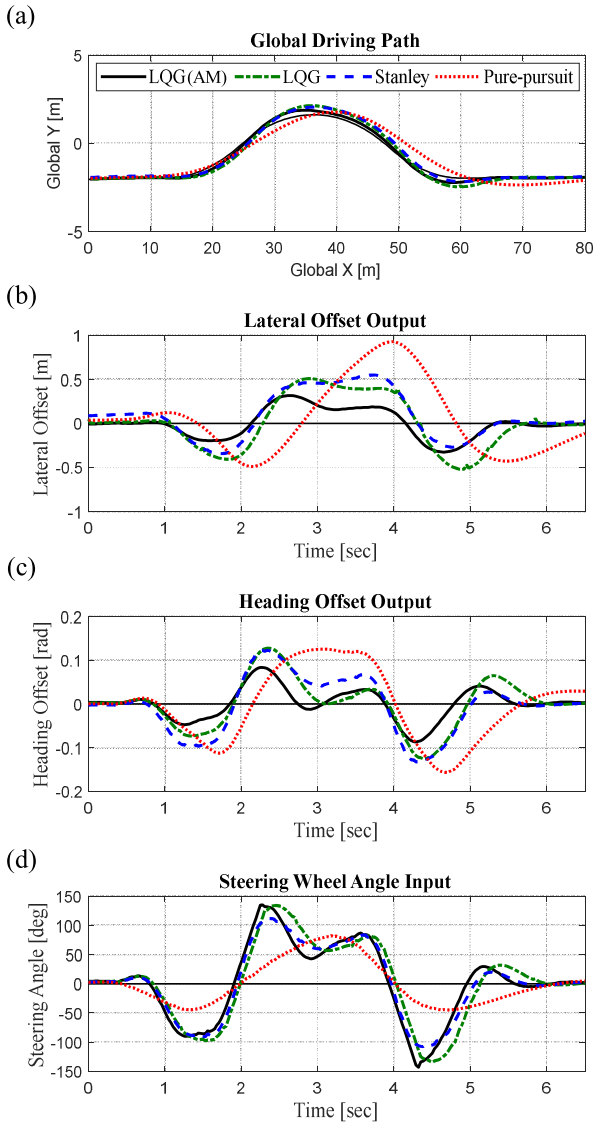

FIGURE 16. Tracking performance experiment results with designed LQG with forward measurement, LQG, Stanley, and Pure-pursuit controllers for DLC test scenario (45kph). (a) Global driving path. (b) Lateral offset, (c) Heading offset, (d) Steering wheel angle.

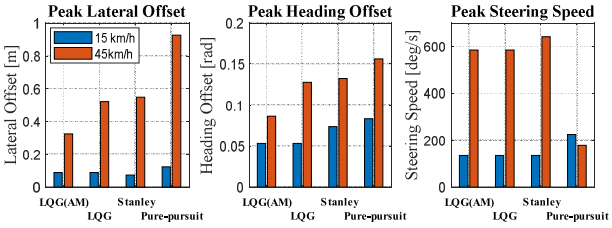

FIGURE 17. Comparison of experiment results (Peak lateral offset, Peak heading offset, Peak steering speed) for DLC test scenario.

state error is reduced by using an adaptive measurement point. The peak lateral offset is within 0.3m, which shows that the tracking performance of this model is better than that of the conventional LQG.

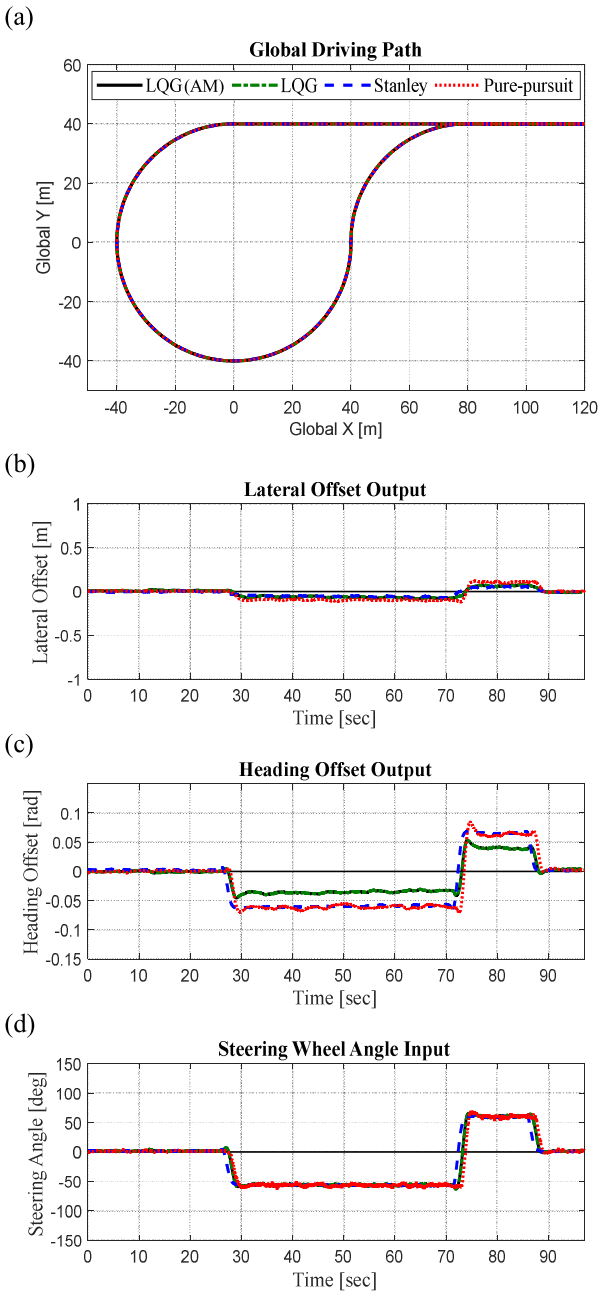

FIGURE 18. Tracking performance experiment results with designed LQG with forward measurement, LQG, Stanley, and Pure-pursuit controllers for constant round test scenario (15kph). (a) Global driving path. (b) Lateral offset, (c) Heading offset, (d) Steering wheel angle.

2) CONSTANT ROUND TEST SCENARIO

The constant round scenario test results at 15kph are shown in Fig. 18. As with the previous DLC experiment results, all controllers show good performance at low speed. The LQG based controllers show heading offset performance better than those of the Stanley and Pure-pursuit methods.

The constant round scenario test results at 45kph are shown in Fig. 19. There is no problem, with all of the controllers simply following the desired path. In the case of the Stanley model, as the speed increases, the lateral offset performance

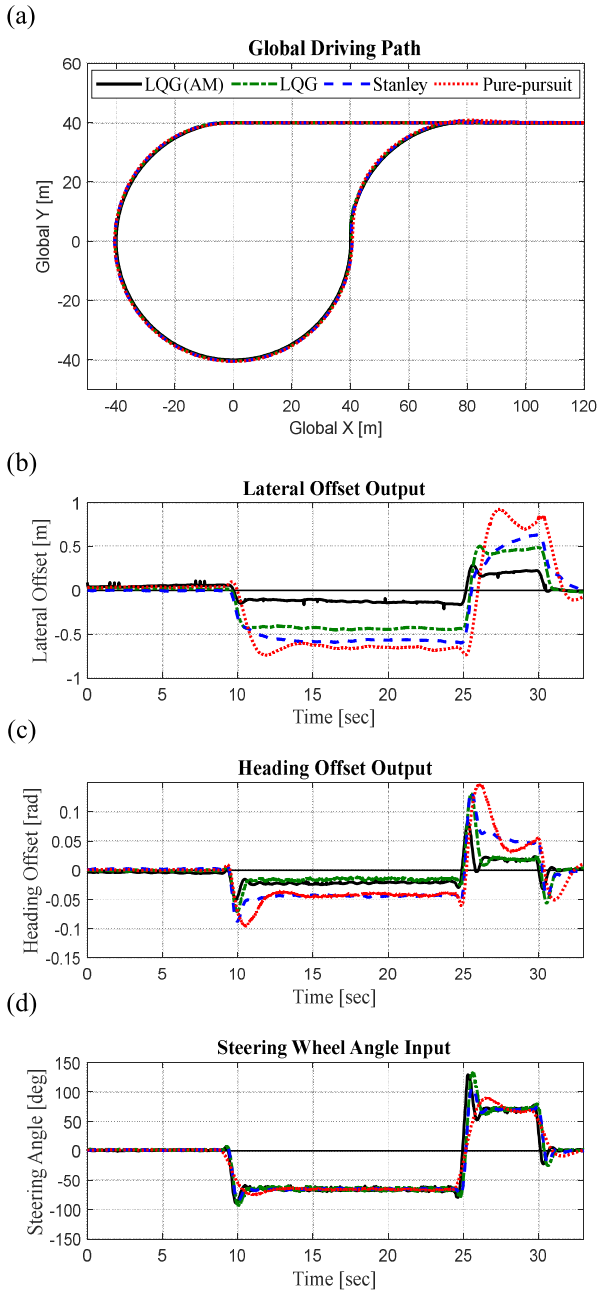

FIGURE 19. Tracking performance experiment results with designed LQG with forward measurement, LQG, Stanley, and Pure-pursuit controllers for constant round test scenario (45kph). (a) Global driving path. (b) Lateral offset, (c) Heading offset, (d) Steering wheel angle.

becomes lower than that of LQG. The Pure-pursuit model showed a large lateral offset, as in the DLC test scenario, and showed a large overshoot with varying curvature. In the case of LQG with AM, the steady state error decreased. This model showed the best performance for the whole driving path.

Quantitative comparison and evaluation results for controller performance are shown in Fig. 20. It can be seen that all controllers have results similar to those in the DLC test scenario. However, as the speed increases in the constant

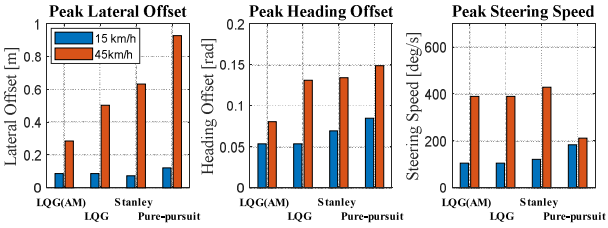

FIGURE 20. Comparison of experiment results (Peak lateral offset, Peak heading offset, Peak steering speed) for constant round test scenario.

round test scenario, the performance starts to vary among controllers. In 15kph results, the peak lateral offset of LQG with AM is lower than 0.3m. On the other hand, in 45kph results, the peak lateral offset values of the Stanley and Pure-pursuit models are larger than 0.6m and 0.9m, respectively. These differences may seem small, but these values are important in determining whether to cross a side lane or not.

The overall tracking characteristics of the controller are similar. It is confirmed that the performance is determined according to the characteristics of each controller irrespective of the test scenario. It is verified that the designed and proposed LQG with AM shows high tracking performance, in addition to full automation according to the vehicle driving speed.

Experimental results show that the performance of LQG using the adaptive Q-matrix is better than those of the other controllers, even if the vehicle speed changes. Also, it was possible to improve the LQG performance by including an adaptive measurement point.

VII. CONCLUSION

An autonomous vehicle tracking controller is designed based on a verified vehicle bicycle model. The designed full-state feedback LQG controller solves the localization and path planning stage problems of error and noise, which occur in actual autonomous vehicle driving.

The design of the observer improved the vibration phenomenon, which could mitigate anxiety and improve the ride comfort of passengers. The two main ideas proposed here played a major role in improving the tracking performance of the controller. The Adaptive Q-matrix showed critical damped tracking performance with no overshoot for all tested vehicle speeds. Use of an adaptive measurement point reduces steady state error at high speed and large curvature driving conditions. Finally, the automatically designed controller showed performance better than those of the Stanley and Pure-pursuit controllers in terms of tracking performance (e.g. lateral offset, heading offset) and passenger comfort, as verified by actual vehicle experiment.

Through this research, autonomous vehicle safety is enhanced via tracking performance improvement, and reduced efforts in tuning for design controller. As future works, it is interesting to consider performance evaluation with other disturbances, e.g., lateral force and moment disturbances and model uncertainties.

APPENDIX

A. STANLEY TRACKING MODEL

The Stanley control method was first used for the Stanley vehicle in the DARPA Grand Challenge [30]. Steering angle is calculated based on the geometry by measuring the lateral offset at the front wheel (e_f). The calculated steering angle is written as Eq. (31).

$$\delta_{stanley} = e_\Psi + tan^{-1}(\frac{k_{stanley} \cdot e_f}{v_x}) \tag{31}$$

where $k_{stanley}$ is the proportional gain for the Stanley controller. In this study, $k_{stanley}$= 0.83 is used in this study.

B. PURE-PURSUIT TRACKING MODEL

The Pure-pursuit tracking model is first discussed in [31]. Several vehicles used this strategy at the DARPA Grand/Urban Challenge [30], [32]. The steering angle is calculated based on the look-ahead distance angle(α), which is followed by a circle to the point where the look-ahead distance(d_{la}) meets the desired path. The calculated steering angle is written as Eq. (32).

$$\delta_{pp} = tan^{-1}\left(\frac{2L \cdot sin\,(\alpha)}{d_{la}}\right) = tan^{-1}(\frac{2L \cdot sin(\alpha)}{k_{pp} \cdot v_x}) \tag{32}$$

where k_{pp} is the proportional gain for the pure-pursuit controller. In this study, k_{pp}= 0.08 is used in this study.

REFERENCES

[1] N. Lyu, C. Deng, L. Xie, C. Wu, and Z. Duan, "A field operational test in China: Exploring the effect of an advanced driver assistance system on driving performance and braking behavior," *Transp. Res. F, Traffic Psychol. Behav.*, to be published. doi: 10.1016/j.trf.2018.01.003.

[2] M. Kyriakidis, C. Weijer, B. Arem, and R. Happee. (2015). *The Deployment of Advanced Driver Assistance Systems in Europe*. [Online]. Available: https://ssrn.com/abstract=2559034

[3] X. Li, Z. Sun, D. Cao, D. Liu, and H. He, "Development of a new integrated local trajectory planning and tracking control framework for autonomous ground vehicles," *Mech. Syst. Signal Process.*, vol. 87, pp. 118–137, Mar. 2017.

[4] Y. Zhang, H. Chen, S. L. Waslander, J. Gong, G. Xiong, T. Yang, and K. Liu, "Hybrid trajectory planning for autonomous driving in highly constrained environments," *IEEE Access*, vol. 6, pp. 32800–32819, 2018.

[5] T. Hesse and T. Sattel, "An approach to integrate vehicle dynamics in motion planning for advanced driver assistance systems," in *Proc. IEEE Intell. Vehicles Symp. (IV)*, Jun. 2007, pp. 1240–1245.

[6] S. Dixit, S. Fallah, U. Montanaro, M. Dianati, A. Stevens, F. Mccullough, and A. Mouzakitis, "Trajectory planning and tracking for autonomous overtaking: State-of-the-art and future prospects," *Annu. Rev. Control*, vol. 45, pp. 76–86, Jan. 2018.

[7] X. Ji, Y. Liu, X. He, K. Yang, X. Na, C. Lv, and Y. Liu, "Interactive control paradigm-based robust lateral stability controller design for autonomous automobile path tracking with uncertain disturbance: A dynamic game approach," *IEEE Trans. Veh. Technol.*, vol. 67, no. 8, pp. 6906–6920, Aug. 2018.

[8] C. Zhang, J. Hu, J. Qiu, W. Yang, H. Sun, and Q. Chen, "A novel fuzzy observer-based steering control approach for path tracking in autonomous vehicles," *IEEE Trans. Fuzzy Syst.*, vol. 27, no. 2, pp. 278–290, Feb. 2019.

[9] Z. Yao, J. Yao, and W. Sun, "Adaptive RISE control of hydraulic systems with multilayer neural-networks," *IEEE Trans. Ind. Electron.*, vol. 66, no. 11, pp. 8638–8647, Nov. 2019.

[10] S. Thrun *et al.*, "Stanley: The robot that won the DARPA grand challenge," *J. Field Robot.*, vol. 23, no. 9, pp. 661–692, Sep. 2006.

[11] G. M. Hoffmann, C. J. Tomlin, M. Montemerlo, and S. Thrun, "Autonomous automobile trajectory tracking for off-road driving: Controller design, experimental validation and racing," in *Proc. Amer. Control Conf.*, Jul. 2007, pp. 2296–2301.

[12] O. Amidi and C. E. Thorpe, "Integrated mobile robot control," *Mobile Robots*, vol. 1388, pp. 504–524, Mar. 1991.

[13] M.-W. Park, S.-W. Lee, and W.-Y. Han, "Development of lateral control system for autonomous vehicle based on adaptive pure pursuit algorithm," in *Proc. 14th Int. Conf. Control, Automat. Syst. (ICCAS)*, Oct. 2014, pp. 1443–1447.

[14] M. Elbanhawi, M. Simic, and R. Jazar, "Receding horizon lateral vehicle control for pure pursuit path tracking," *J. Vib. Control*, vol. 24, no. 3, pp. 619–642, Feb. 2018.

[15] S. Hahn, K. Zindler, K. Doll, and U. Jumar, "New control scheme for a lane-keeping evasive maneuver exploiting the free space optimally," in *Proc. 20th Int. Conf. Methods Models Automat. Robot. (MMAR)*, Aug. 2015, pp. 856–861.

[16] J. Kong, M. Pfeiffer, G. Schildbach, and F. Borrelli, "Kinematic and dynamic vehicle models for autonomous driving control design," in *Proc. IEEE Intell. Vehicles Symp. (IV)*, Jun./Jul. 2015, pp. 1094–1099.

[17] Y. Xia, F. Pu, S. Li, and Y. Gao, "Lateral path tracking control of autonomous lane vehicle based on ADRC and differential flatness," *IEEE Trans. Ind. Electron.*, vol. 63, no. 5, pp. 3091–3099, May 2016.

[18] M. Brown, J. Funke, S. Erlien, and J. C. Gerdes, "Safe driving envelopes for path tracking in autonomous vehicles," *Control Eng. Pract.*, vol. 61, pp. 307–316, Apr. 2017.

[19] J. Funke, M. Brown, S. M. Erlien, and J. C. Gerdes, "Collision avoidance and stabilization for autonomous vehicles in emergency scenarios," *IEEE Trans. Control Syst. Technol.*, vol. 25, no. 4, pp. 1204–1216, Jul. 2016.

[20] J. Ji, A. Khajepour, W. W. Melek, and Y. Huang, "Path planning and tracking for vehicle collision avoidance based on model predictive control with multiconstraints," *IEEE Trans. Ultrason. Eng.*, vol. 66, no. 2, pp. 952–964, Feb. 2017.

[21] H. Guo, D. Cao, H. Chen, Z. Sun, and Y. Hu, "Model predictive path following control for autonomous cars considering a measurable disturbance: Implementation, testing, and verification," *Mech. Syst. Signal Process.*, vol. 118, pp. 41–60, Mar. 2019.

[22] Q. Cui, R. Ding, B. Zhou, and X. Wu, "Path-tracking of an autonomous vehicle via model predictive control and nonlinear filtering," *Proc. Inst. Mech. Eng. D, J. Automobile Eng.*, vol. 232, no. 9, pp. 1237–1252, 2017.

[23] R. Marino, S. Scalzi, and M. Netto, "Nested PID steering control for lane keeping in autonomous vehicles," *Control Eng. Pract.*, vol. 19, no. 12, pp. 1459–1467, 2011.

[24] P. Zhao, J. Chen, Y. Song, X. Tao, T. Xu, and T. Mei, "Design of a control system for an autonomous vehicle based on adaptive-PID," *Int. J. Adv. Robotic Syst.*, vol. 9, no. 2, p. 44, Jul. 2012.

[25] C. Hu, H. Jing, R. Wang, F. Yan, and M. Chadli, "Robust H∞ output-feedback control for path following of autonomous ground vehicles," *Mech. Syst. Signal Process.*, vols. 70–71, pp. 414–427, 2016.

[26] H. Jing, C. Hu, F. Yan, M. Chadli, R. Wang, and N. Chen, "Robust H_∞ path following control for autonomous ground vehicles with delay and data dropout," *IEEE Trans. Intell. Transp. Syst.*, vol. 17, no. 7, pp. 2042–2050, Jul. 2016.

[27] D. J. Cole, A. J. Pick, and A. M. C. Odhams, "Predictive and linear quadratic methods for potential application to modelling driver steering control," *Vehicle Syst. Dyn.*, vol. 44, no. 3, pp. 259–284, 2006.

[28] S. Xu and H. Peng, "Design, analysis, and experiments of preview path tracking control for autonomous vehicles," *IEEE Trans. Intell. Transp. Syst.*, to be published. doi: 10.1109/TITS.2019.2892926.

[29] J. Jiang and A. Astolfi, "Lateral control of an autonomous vehicle," *IEEE Trans. Veh. Technol.*, vol. 3, no. 2, pp. 228–237, Jun. 2018.

[30] R. Rajamani, H.-S. Tan, B. K. Law, and W.-B. Zhang, "Demonstration of integrated longitudinal and lateral control for the operation of automated vehicles in platoons," *IEEE Trans. Control Syst. Technol.*, vol. 8, no. 4, pp. 695–708, Jul. 2000.

[31] M. Buehler, K. Iagnemma, and S. Singh, *The 2005 DARPA Grand Challenge: The Great Robot Race*, vol. 36. New York, NY, USA: Springer, 2007.

[32] R. Wallace, A. Stentz, C. E. Thorpe, H. P. Maravec, W. Whittaker, and T. Kanade, "First results in robot road-following," in *Proc. 9th Int. Joint Conf. Artif. Intell.*, Aug. 1985, pp. 1089–1095.

[33] M. Buehler, K. Iagnemma, and S. Singh, *The DARPA Urban Challenge: Autonomous Vehicles in City Traffic*, vol. 56. New York, NY, USA: Springer, 2009.

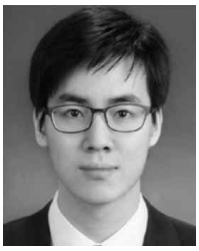

KIBEOM LEE received the master's degree from the Korea Advanced Institute of Science and Technology (KAIST), Daejeon, South Korea, in 2014, where he is currently pursuing the Ph.D. degree. His research interests include the fields of vehicle dynamics, advanced driver assist systems, control, and autonomous vehicles.

SEUNGMIN JEON received the bachelor's degree from Sungkyunkwan University, Suwon, South Korea, in 2018. He is currently pursuing the master's degree with the Korea Advanced Institute of Science and Technology (KAIST), Daejeon, South Korea. His research interests include the fields of vehicle dynamics, advanced driver assist systems, control, and autonomous vehicles.

HEEGWON KIM received the master's degree from Hanyang University, Seoul, South Korea, in 2009. He is currently with Hyundai Motor Company (HMC), Gyeonggi-Do, South Korea. His research interests include the fields of vehicle dynamics, advanced driver assist systems, and vehicle control.

DONGSUK KUM received the Ph.D. degree in mechanical engineering from the University of Michigan, Ann Arbor, in 2010.

He was with the General Motors R&D Propulsion Systems Research Laboratory, Warren, MI, USA, as a Visiting Research Scientist. His works at General Motors focused on advanced propulsion system technologies, including hybrid electric vehicles, flywheel hybrid, and waste heat recovery systems. He is currently an Assistant Professor with The Graduate School of Green Transportation, Korea Advanced Institute of Science and Technology (KAIST), and the Director of the Vehicular Systems Design and Control (VDC) Laboratory. His research interests include the modeling, control, and design of advanced vehicular systems with particular interests in hybrid electric vehicles and autonomous vehicles.